Brightness Equalization Algorithm for Chinese Painting Pigments in Low-Light Environment Based on Region Division

Lijuan Cheng
College of Art and Art Design, Henan Vocational University of Science and Technology, Zhoukou, 466000, China

***Abstract*—With the promotion and development of Chinese painting and the advancement of photography technology, people can appreciate various types of Chinese paintings through image and other methods. However, Chinese painting images in low-light environments face the problem of extreme uneven brightness distribution. The currently proposed solutions for this problem are not sufficient. Therefore, this research proposes a brightness equalization algorithm for Chinese painting pigments in low-light environments based on region division. This algorithm also utilizes guided filtering for image denoising. In performance testing, the proposed method has a runtime of 16.63 seconds under a scaling factor of 1 and a runtime of 8.37 seconds under a scaling factor of 0.1, which are the fastest among the compared algorithms. In simulation experiments, the brightness equalization value of the proposed method is 198.93, which is listed at the best among all the compared algorithms. This research provides a valuable research direction for the brightness equalization of Chinese painting pigments.**

***Keywords*—Chinese painting; low-light; region division; guided filtering; scaling factor**

I. Introduction

In the process of promoting Chinese painting, pigments are one of the most visually impactful elements for viewers, as they directly determine the visual effects of the artwork [1]. However, due to the limitations of low-light environments, Chinese paintings in low-light scenes may face the problem of uneven pigment brightness, which affects the visibility and artistic quality of the artwork to some extent. A low-light environment refers to an environment with dim lighting or insufficient light sources [2]. In such environments, due to the scarcity and weakening of light, details in the image are difficult to display clearly, and the differences in pigment brightness become more pronounced. This significantly affects the appreciation of Chinese paintings by viewers. At present, the processing methods for low light images include image enhancement, noise removal, and multi frame image fusion, which can be divided into two approaches: hardware and software. However, the focus is mainly on software upgrades and improvements [3]. Due to the uneven lighting in the shooting environment, the brightness of captured images may be uneven, with some areas appearing too bright while others are too dark. Existing brightness equalization algorithms not only enhance the noise in the image but also have issues with inconsistent equalization across different regions [4].

Therefore, this research proposes a brightness equalization algorithm for Chinese painting pigments in low-light environments based on region division. This study will provide reference and guidance for the application of region-based brightness equalization algorithms in the field of Chinese painting pigment brightness equalization and other related fields. The research is divided into five sections: an overview of the research in Section I, a review of domestic and foreign studies in Section II, a study on the algorithm's methodology in Section III, performance testing of the algorithm in Section IV, and a summary and outlook on the limitations of this research in Section V.

II. Literature Review

Researchers have focused on using image region division techniques to improve image enhancement methods. Matsuyama E proposed a segmentation method for chest X-ray images. This method can automatically remove the scapular region, mediastinal region, and diaphragm region from various chest X-ray images as the learning data for this method. The method uses a simple linear iterative clustering algorithm and local entropy filtering to generate an entropy map, which is then subjected to morphological operations to perform region segmentation on the lung image. The method was tested, and the results showed that it can remove non-pulmonary markings from the image and present clear X-ray images of the lungs [5]. Chen et al. found that the evaluation metrics of existing iris segmentation algorithms may be influenced by inaccurate localization of the Ground Truth image. Therefore, researchers proposed using a mask image segmented based on deep learning algorithms as a substitute for the Ground Truth image. Experimental results showed that the mask image segmented based on deep learning algorithms can completely replace the original Ground Truth image [6]. Cao et al. found that existing line art coloring methods can produce credible coloring results, but these methods are often affected by color bleeding issues. Therefore, researchers proposed an explicit segmentation fusion mechanism. Testing outcomes shows that the model can better fulfill the coloring instructions given by the user and can greatly alleviate the problem of color bleeding artifacts [7].

Image enhancement methods are applicable in various fields, and researchers have made many improvements to these methods. Tirumani et al. found that existing image enhancement methods have unstable effects on contrast and resolution enhancement. Therefore, researchers process the

resolution of the image, and then used auto optimization to enhance the resolution and brightness. Testing outcomes showed that this method can effectively and stably enhance the resolution and contrast of the image [8]. Xu et al. proposed a multi-scale fusion framework for low-light image enhancement. This framework first generates multiple artificially multi-exposure images using a mapping function, then combines exposure to create a weight map, and finally fuses different frequency bands of the image. Testing outcomes showed that this method outperforms existing algorithms in enhancing low-light images [9]. Lu et al. believed that the current image enhancement methods based on convolutional neural network models do not differentiate image features on different channels, which hinders the learning of hierarchical features. Therefore, researchers proposed a channel-split attention network that can analyze shallow features in a targeted manner by splitting them into residual and dense branches. Experimental results showed that this method exhibited excellent performance in both qualitative and quantitative evaluations [10].

In summary, although region division methods have been applied in multiple fields, their combination with image enhancement for brightness equalization of Chinese painting pigments is relatively rare. Therefore, this research proposes a brightness equalization algorithm for Chinese painting pigments in low-light environments based on region division, providing effective technical support for the promotion of Chinese painting.

III. Region-based Brightness Equalization Algorithm for Chinese Painting Pigments in Low-Light Environments

Chinese painting images in low-light environments often suffer from uneven lighting in the pigment display [11]. Traditional image brightness equalization algorithms have limitations in achieving sufficient brightness equalization and enhancing all local details [12]. To address this issue, this research proposes a region-based brightness equalization algorithm for Chinese painting pigments in low-light environments. This algorithm improves existing image enhancement algorithms and provides effective assistance in the refinement of image enhancement algorithms.

A. Single-Frame Image Brightness Equalization Enhancement Method in Low-Light Environments

Images in image processing come in various formats, including RGB, LAB, YUV, HSV, HIS, etc. The main image format studied in this research is HSV. In this research, the RGB image is first converted to the HSV image. In HSV, H represents the hue of the image, S represents the saturation, and V represents the value or brightness of the image. The advantage of the HSV format is that the color information of the image does not affect the brightness component, which ensures that the original colors of the image are preserved during brightness enhancement. The schematic diagram of an HSV image is shown in Fig. 1.

In Fig. 1, a cone shape is hired to manifest the HSV color space, where the hue is determined by the rotation angle around the center of the cone, with each 120° representing a different color. The closer to the center of the cross-section, the less saturated the color is, and the closer to the apex of the cone, the weaker the brightness. The conversion of RGB to HSV is represented by Eq. (1).

$$V = \max\{R, G, B\} \tag{1}$$

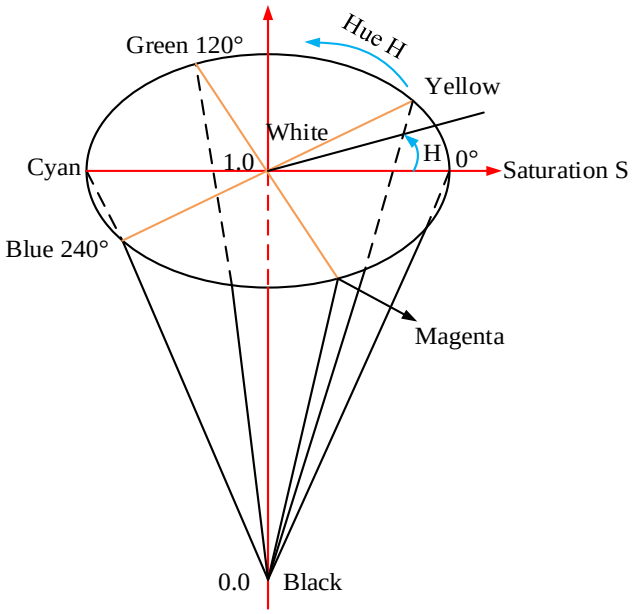

Fig. 1. The schematic diagram of an HSV image.

In Eq. (1), R, G, B represent the three primary colors in the RGB color space, where R means red, B represents blue, and G represents green. The converted S value is represented by Eq. (2).

$$S = \begin{cases} \dfrac{V - \min\{R, G, B\}}{V}, V \neq 0 \\ 0, otherwise \end{cases} \tag{2}$$

In Eq. (2), V represents the value obtained from Eq. (1). The converted H value is represented by Eq. (3).

$$H = \begin{cases} 0°, V = \min(R, G, B) \\ 60° \times \dfrac{G - B}{(V - \min(R, G, B))} + 0°, V = R, G \geq B \\ 60° \times \dfrac{G - B}{(V - \min(R, G, B))} + 360°, V = R, G < B \\ 60° \times \dfrac{G - B}{(V - \min(R, G, B))} + 120°, V = G \\ 60° \times \dfrac{G - B}{(V - \min(R, G, B))} + 240°, V = B \end{cases} \tag{3}$$

In Eq. (3), R represents the R value in the RGB. The brightness of an HSV image is divided into different levels [13]. The average brightness range of the V channel is $[0,1]$. An empirical threshold I_{th} is set, and when the average brightness of an image is below this threshold, the image is

considered a high-brightness image. Therefore, the brightness range of high-brightness images is $[I_{th},1]$. For the enhancement of high-brightness images, the focus is mainly on enhancing the contrast [14]. Since the enhancement results of high-brightness images are similar to those of low-brightness images, this research converts high-brightness images to low-brightness images for enhancement and then converts them back to high-brightness images after enhancement [15]. The formula for obtaining the limited brightness image is represented by Eq. (4).

$$I_{\lim} = \begin{cases} I_v, \overline{I_v} \le I_{th} \\ 1 - I_v, \overline{I_v} > I_{th} \end{cases} \tag{4}$$

In Eq. (4), $I_{\lim}$ represents the limited brightness channel image, I_v represents the V channel image extracted after converting from RGB to HSV, and $\overline{I_v}$ represents the average brightness of the V channel image. The brightness region division of the image in this research is divided into four steps. The first step is the initial enhancement of the limited V channel image, and the enhancement formula is represented by Eq. (5).

$$F = \log_2(1 + I_{\lim}) \tag{5}$$

In Eq. (5), $I_{\lim}$ represents the limited V channel image, and F represents the image after initial enhancement. The region segmentation of the image in this research is divided into four steps. The second step is the binarization of the multi-scale image [16]. Two different binarization methods are used for the edges and region shapes of the image. The first binarization method first applies mean filtering to the image F after initial enhancement to obtain the neighborhood mean value of each pixel. Then, the brightness value is divided by the neighborhood mean value, and the result is compared with the adaptive sensitivity factor T. Finally, the binarized V channel brightness image is obtained. The calculation process is represented by Eq. (6).

$$F_{binary\_1}(x,y) = \begin{cases} 1, \dfrac{F(x,y)}{F_{s1\times s1}(x,y)} > T \\ 0, otherwise \end{cases} \tag{6}$$

In Eq. (6), $F(x,y)$ represents the brightness value of each pixel, and $F_{s1\times s1}(x,y)$ represents the neighborhood mean value. The second binarization method subtracts the mean filtering image from F, and then subtracts a constant C to obtain the difference image I_{sm}. Then, based on the pixel values of I, binarization is performed to obtain a binary image containing texture boundaries. The calculation process is represented by Eq. (7).

$$F_{binary\_2}(x,y) = \begin{cases} 1, I_{sm}(x,y) > 0 \\ 0, otherwise \end{cases} \tag{7}$$

In Eq. (7), $I_{sm}(x,y)$ represents the pixel values of the image I_{sm}. The second step of region image processing is fusion, which involves merging the two binarized images obtained earlier to create a new binary image. The fusion formula is shown in Eq. (8).

$$F_{binary} = F_{binary\_1} \oplus F_{binary\_2} \tag{8}$$

In Eq. (8), $\oplus$ represents the logical AND operator. The third step is noise reduction using morphology. The fourth step is region segmentation. The specific operation involves first marking the boundaries of the denoised regions, and then dividing the image into multiple regions and assigning them numbers based on the marked content. The schematic diagram of image segmentation is shown in Fig. 2.

In Fig. 2, the images from left to right are the original image, the two binarized images, the fused image obtained from the fusion calculation of the two binarized images, the denoised binary image, and the segmented image. Due to the significant brightness differences between different regions in images with uneven lighting, targeted brightness adjustment is needed [17]. The image is marked based on the different brightness levels in different regions, and the marking rule is shown in Eq. (9).

$$\begin{cases} if \dfrac{(V_{i\min} + V_i)}{2} > 0.5, bright \\ else, dark \end{cases} \tag{9}$$

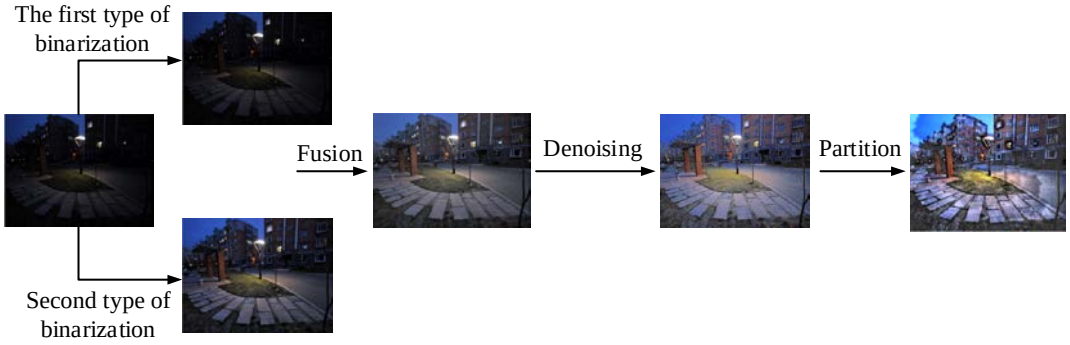

Fig. 2. Schematic diagram of image partitioning.

In Eq. (9), i represents the index of the region, $V_{i\min}$ represents the minimum brightness value in that region, and $\overline{V_i}$ represents the average brightness of that region.

B. Image Brightness Equalization Enhancement Method Based on Region Denoising

Denoising is an important step in image enhancement. Currently, there are various denoising methods, including bilateral filtering-based denoising, Gaussian filtering-based denoising, and linear guided filtering-based denoising [18]. The denoising method based on bilateral filtering is computationally complex and slow. The denoising method based on Gaussian filtering tends to blur the edges of the denoised image and result in unclear presentation of image details. The denoising method based on linear guided filtering produces clear edges in the denoised image without artifacts and has a faster computation speed. Therefore, in this research, the guided filtering method is used for image denoising. The workflow of the guided filtering denoising method is shown in Fig. 3.

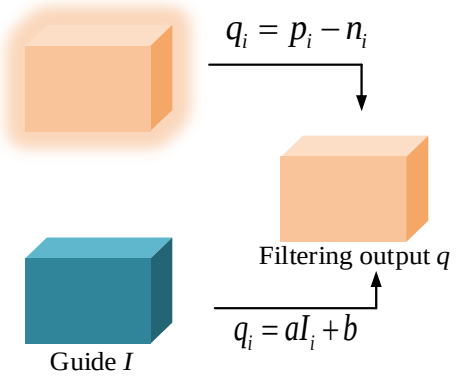

Fig. 3. Guiding the workflow of filtering and noise reduction methods.

In Fig. 3, the workflow of guided filtering includes a guidance image I, an input image p, and an output image q. The guidance image can be pre-set based on different application scenarios, but it can also be replaced by the input image. The guided filtering principle is based on the premise assumption that a linear relationship exists between the guidance image and the output image. Assuming that in a window ω_m centered at pixel m, q is a linear transformation of I, the transformation formula is shown in Eq. (10).

$$q_i = a_m I_i + b_m, \forall i \in \omega_m \tag{10}$$

In Eq. (10), a_m and b_m represent the assumed linear invariant coefficients within the window ω_m, and ω_m is a square window with a radius of r centered at pixel m. To determine the values of a_m and b_m, constraints need to be applied to the input image p, and the constraints are shown in Eq. (11).

$$q_i = p_i - n_i \tag{11}$$

In Eq. (11), n represents the excess information in q, where most of the irrelevant information is noise. The linear regression model established in window ω_m is shown in Eq. (12).

$$E(a_m, b_m) = \sum_{i \in \omega_m} ((a_m I_i + b_m - p_i)^2 + \varepsilon a_m{}^2 \tag{12}$$

In Eq. (12), ε is a regularization parameter to constrain a_m, and its solution is shown in Eq. (13).

$$\begin{cases} a_m = \dfrac{\frac{1}{|\omega|}\sum_{i \in \omega_m} I_i p_i - \mu_m \overline{p}_m}{\sigma_m{}^2 + \varepsilon} \\ b_m = \overline{p}_m - a_m \mu_m \end{cases} \tag{13}$$

In Eq. (13), $\sigma_k{}^2$ and μ_k represent the variance and mean of I within window ω_m, $|\omega|$ represents the number of pixels in ω_m, and $\overline{p}_m = \frac{1}{|\omega|}\sum_{i \in \omega_m} p_i$ represents the mean of p within window ω_m. Since pixel i is included in different ω_m, there will be multiple values of q_i in different windows. Therefore, Eq. (14) is used to determine the value of q_i.

$$q_i = \frac{1}{|\omega|}\sum_{m|i \in \omega_m} (a_m I_i + b_m) = \overline{a}_m I_i + b_m \tag{14}$$

Due to the rotational symmetry property of the summation window, $\sum_{m|i \in \omega_m} a_m = \sum_{i|m \in \omega_i} a_m$ can be obtained. Therefore, Eq. (14) can also be written as Eq. (15).

$$q_i = \overline{a}_i I_i + \overline{b}_i \tag{15}$$

In Eq. (15), $\overline{a}_i = \frac{1}{|\omega|}\sum_{m \in \omega_i} a_m$ and $\overline{b}_i = \frac{1}{|\omega|}\sum_{m \in \omega_i} b_m$ represent the mean of the calculated results of the linear coefficients for pixel i. The denoising effects of different denoising methods on the same image are shown in Fig. 4.

In Fig. 4, Fig. 4(b) is the image after denoising with Gaussian filtering, Fig. 4(c) is the image after denoising with bilateral filtering, and Fig. 4(d) is the image after denoising with guided filtering. Fig. 4(a) is the original one. The image after denoising with Gaussian filtering appears darker in color and has unclear edges. The image after denoising with bilateral filtering has clear brightness edges. The image after denoising with guided filtering has clear brightness edges and the details in each region are smoothed, which better matches the actual lighting distribution [19]. In order to achieve better enhancement of the image, this research uses a two-dimensional gamma function to perform brightness correction on images with uneven lighting [20]. The formula for the two-dimensional gamma function is shown in Eq. (16).

$$I_g(x,y)=255\times\left(\frac{F(x,y)}{255}\right)^{\gamma},\gamma=M(x,y)^{\frac{M(x,y)-I_q(x,y)}{M(x,y)}} \quad (16)$$

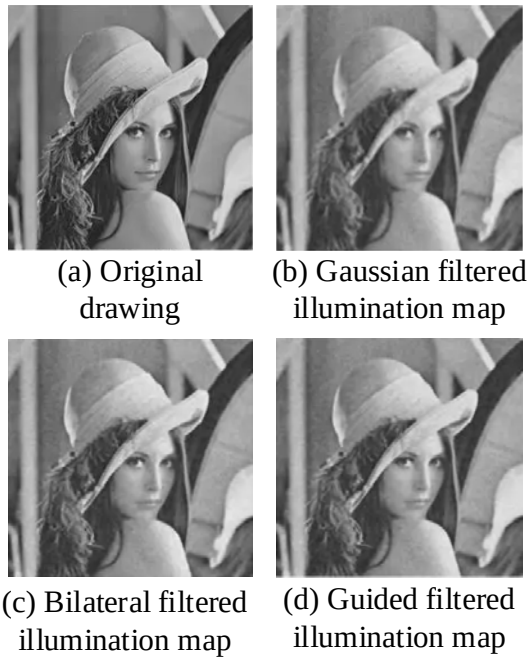

Fig. 4. Noise reduction effect diagram.

In Eq. (16), F represents the preliminarily enhanced image after transformation, I_g represents the output enhanced image, M represents the target mean, and $I_g(x,y)$ represents the image after denoising with guided filtering. When $M(x,y)>I_q(x,y)$ I, $\gamma<1$, indicating an increase in brightness for $F(x,y)$; otherwise, the brightness is reduced. The image obtained is further filtered using guided filtering with a radius of six and a regularization parameter of $1e-4$ for denoising. Then, contrast-limited histogram equalization is applied to obtain the image I_c, which is then weighted fused using the weighted fusion formula shown in Eq. (17).

$$I_{out}=a\cdot I_c+b\cdot I_g,\begin{cases}a=\begin{cases}0.5+0.1\times\dfrac{\mu(I_v)-0.4}{0.6},\mu(I_v)\geq 0.4\\ 0.5,else\end{cases}\\ b=1-a\end{cases} \quad (17)$$

In Eq. (17), a represents the weighting coefficient for the output of contrast-limited histogram equalization, b represents the weighting coefficient for I_g, and $\mu(I_v)$ represents the mean brightness of the V channel image of the original image. Finally, the I_{out} channel image, the H (hue) channel image I_H from the initial input image, and the S (saturation) channel image I_S are combined to form an HSV image, which is then converted to the RGB format and output as the final RGB image. In summary, the workflow of the brightness equalization algorithm based on region division in low-light conditions is shown in Fig. 5.

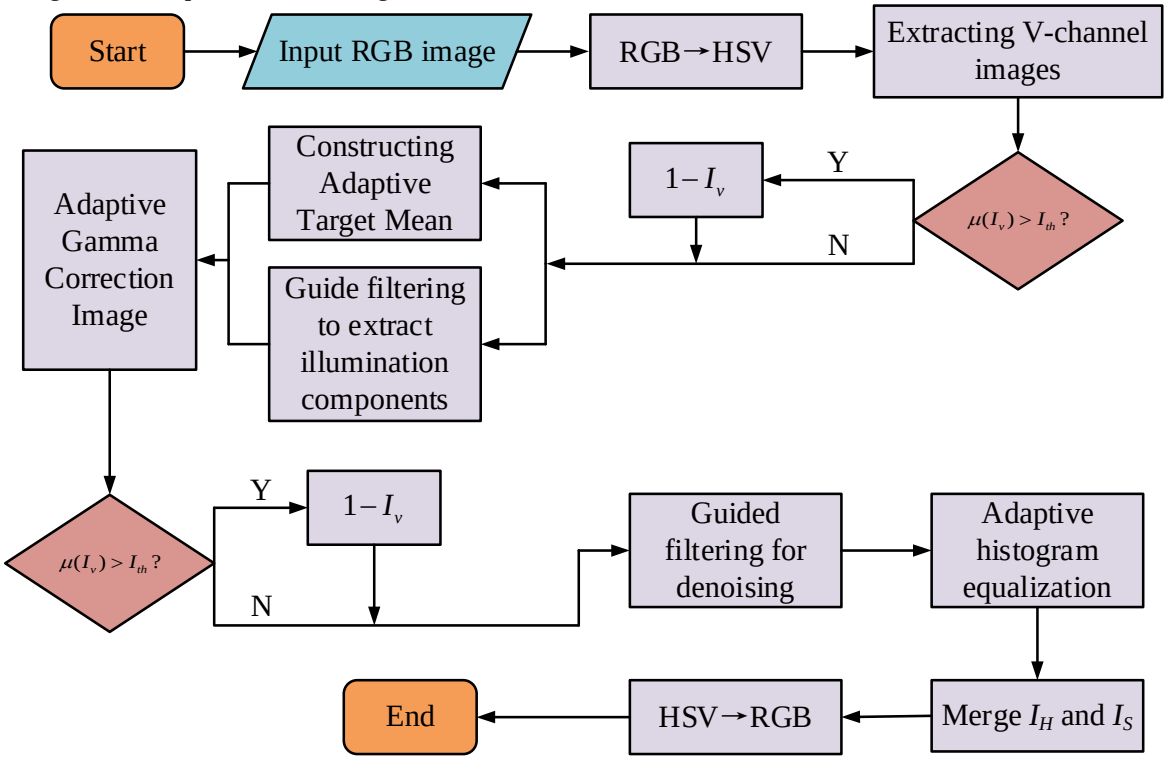

Fig. 5. Flow chart of brightness equalization algorithm for Chinese painting pigments in low illumination environments based on region division.

In Fig. 5, the first step is to input the original image in RGB format. The second step is to convert the original RGB image to the HSV format and extract the V channel image I_V. The third step is to calculate the grayscale mean of image I_V and determine if the mean is greater than a set empirical threshold I_{th}. If the mean is less than I_{th}, the mean remains unchanged. If the mean is greater than I_{th}, the mean is inverted, resulting in a mean-limited grayscale image $I_{\lim}$. The fourth step consists of three operations. The first operation is logarithmic transformation followed by binarization to obtain a binary image containing texture edges. Then, the binary image is segmented into regions. The second operation is 8-neighborhood mean filtering to obtain neighborhood information for each pixel. The third operation is denoising of the grayscale image $I_{\lim}$ using guided filtering, resulting in an illumination map I_q. The fifth step of the algorithm is to construct the target mean M_i for each region based on the brightness mean, minimum value, and image mean of the original input image within the regions segmented in the first operation of the fourth step. The sixth step is to perform gamma correction on the preliminarily enhanced image to achieve brightness correction, resulting in the image I_g. The seventh step is to determine whether the inversion operation was performed in the third step. If inversion was performed, the image I_g is restored; if not, it remains unchanged. The eighth step is to denoise the image I_g using guided filtering to obtain the denoised image. The ninth step is to perform contrast-limited histogram equalization on I_g and then perform weighted fusion to obtain the corrected image I_{out}. The final step is to combine the H and S channels back into the HSV color space, convert it to RGB format, and output the brightness equalized image.

IV. Performance Analysis and Simulation Experiment of Region-based Image Brightness Equalization Algorithm

A. Performance Analysis of Region-based Image Brightness Equalization Algorithm

The processor used for this performance test is an Intel(R) Core (TM) i9-13900HX CPU with a clock speed of 5.4GHz, 16GB RAM, and a 64-bit operating system. The simulation software used is MATLAB R2022a. The images used in this experiment were obtained by continuously capturing 300 frames of the same Chinese painting in a low-light indoor environment. Five frames were randomly selected from the 300 frames of Chinese painting images and named Frame 1 to 5. The information entropy and Structural Similarity (SSIM) of the images enhanced by different algorithms were compared. The comparison of information entropy is Table I.

From Table I, the original images information entropy is generally in the range of 4-6. After MSRCR processing, it is in the range of 5-7. After Dong processing, the information entropy is in the range of 6-8. After Zohair processing, the information entropy is in the range of 7-9. After processing with the proposed method, the information entropy of the images is in the range of 9-10. A higher information entropy value indicates more detailed information in the image. The images processed by the proposed algorithm in this study show significantly more detailed information compared to other algorithms. The comparison results of SSIM are shown in Table II.

TABLE I. Information Entropy

Algorithm	Frame 1	Frame 2	Frame 3	Frame 4	Frame 5
Original drawing	4.63	5.55	5.16	4.86	5.03
MSRCR	6.36	5.98	5.66	5.13	6.05
Dong	7.32	6.98	7.55	6.77	7.09
Zohair	7.53	8.25	7.86	8.03	7.33
This study	9.56	9.43	9.36	9.78	9.89

TABLE II. Structural Similarity Comparison Results

Algorithm	Frame 1	Frame 2	Frame 3	Frame 4	Frame 5
MSRCR	0.06	0.13	0.22	0.09	0.23
Dong	0.23	0.15	0.09	0.21	0.26
Zohair	0.22	0.26	0.19	0.23	0.25
This study	0.30	0.34	0.29	0.36	0.35

From Table II, the SSIM of the images reinforced by MSRCR is in the range of 0.06-0.23. The SSIM of the images enhanced by Dong is in the range of 0.09-0.26. The SSIM of the images enhanced by Zohair is in the range of 0.19-0.26. The SSIM of the images enhanced by the proposed method in this study is in the range of 0.30-0.36. The SSIM of the images enhanced by the method is significantly higher than other algorithms, indicating that the details of the images preserved by the method are more complete and the enhancement effect is better compared to other algorithms. A comparison was made between the adaptive gamma brightness correction method used in the algorithm and the fixed parameter gamma correction method. The experimental results are shown in Fig. 6.

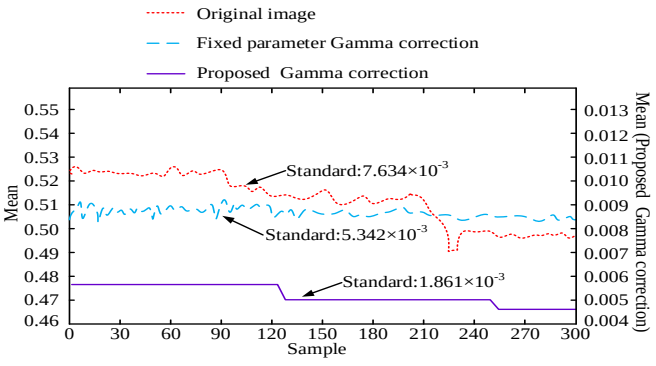

Fig. 6. Comparison of different gamma brightness correction methods.

In Fig. 6, from the experimental results, it can be observed that when the input images are in the range of 1-300 frames, the brightness fluctuation of the images corrected by the

improved adaptive gamma correction method in this study significantly decreases compared to the original images. On the other hand, the images corrected by the fixed parameter gamma correction method exhibit larger brightness fluctuations compared to the original images. The adaptive gamma correction method used in this study outputs a standard deviation of brightness of 1.861×10^{-3}, while the original images have a brightness standard deviation of 7.634×10^{-3}, and the images corrected by the fixed parameter gamma correction method have a brightness standard deviation of 5.342×10^{-3}. The standard deviation of brightness corrected by the adaptive gamma correction method is significantly lower than that of the original images and the fixed parameter gamma correction method. This study also compared the runtime of different algorithms at different scaling factors. The specific results are shown in Fig. 7.

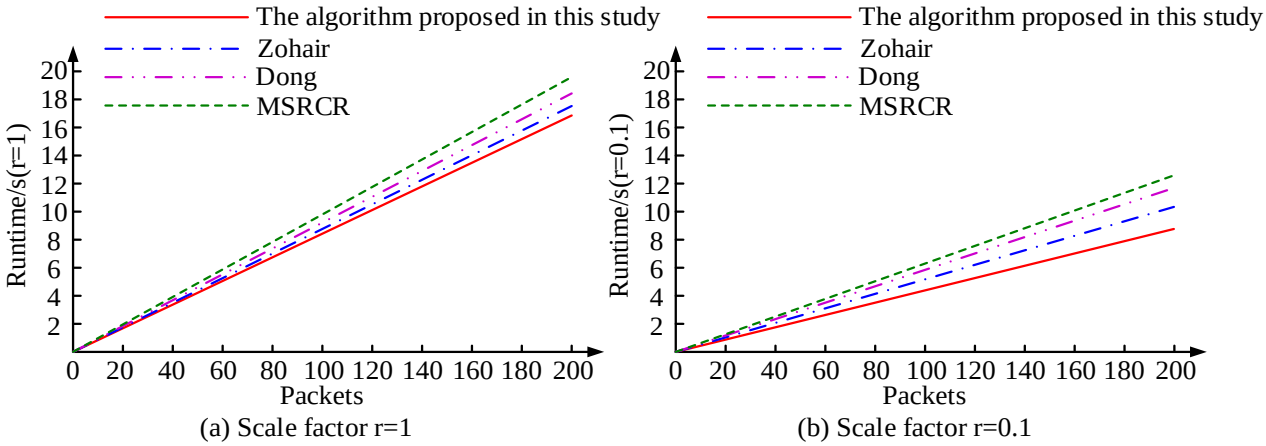

Fig. 7. Running time of different algorithms under different scaling coefficients.

Fig. 7(a) represents the runtime of different algorithms with varying group numbers under a scaling factor of 1. It can be observed that under a scaling factor of 1, the runtime of all algorithms increases with the increase in group numbers. When the group number reaches 200, the proposed algorithm in this study has the shortest runtime among all algorithms, which is 16.63 seconds. Fig. 7(b) represents the runtime of different algorithms with varying group numbers under a scaling factor of 0.1. It can be seen that under a scaling factor of 0.1, the runtime of all algorithms is significantly shorter compared to the case of a scaling factor of 1. Among them, the proposed algorithm in this study has the shortest runtime among all group numbers, which is 8.37 seconds when the group number reaches 200.

B. Simulation Experiment of Brightness Equalization Algorithm for Chinese Painting Images Based on Regional Division

The comparison of the average brightness of Chinese painting pigments enhanced by different enhancement algorithms in low-light environments is shown in Fig. 8.

In Fig. 8, the image enhanced by the MSRCR image enhancement algorithm has the lowest average brightness among the five algorithms, indicating that its brightness equalization processing is the worst among the five algorithms. The image enhanced by the Dong image enhancement algorithm has a lower average brightness and a slower growth rate. The image enhanced by the Zohair image enhancement algorithm has a higher average brightness and a faster growth rate. The image enhanced by the algorithm proposed maintains a high level of average brightness and has a fast growth rate. This study introduced the Peak Signal-to-Noise Ratio (PSNR) for evaluating the fidelity of the images. PSNR tests were conducted on different algorithms using the Brightening dataset and the LOL dataset, and the results are shown in Fig. 9.

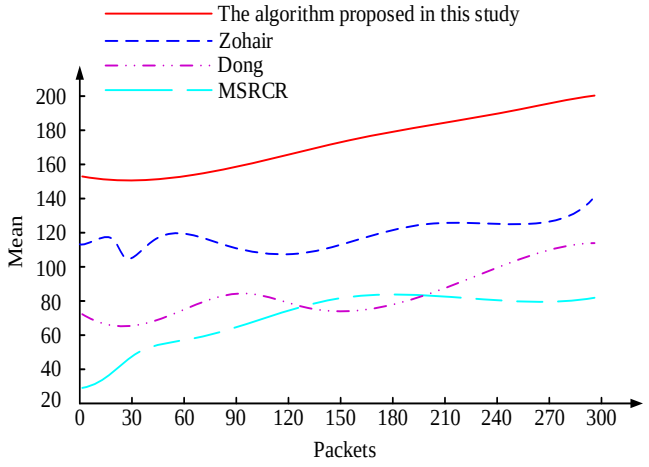

Fig. 8. Average brightness results of Chinese painting pigments in low illuminance environments with different enhancement algorithms for image enhancement.

In Fig. 9, Fig. 9(a) shows the comparison of PSNR for different algorithms under the Brightening dataset. The PSNR of the MSRCR algorithm is close to that of the Dong algorithm, and both algorithms have large fluctuations. The PSNR of the Zohair algorithm is higher, and its fluctuations are more stable than the above two algorithms. The PSNR of the algorithm proposed is greater than the above three at bit rates ranging from 0 to 2000, and it has a fast growth rate. The maximum PSNR values for the four algorithms are obtained when the bit rate reaches 2000, which are 26.6db, 28.4db,

32.5db, and 37.6db, respectively. Fig. 9(b) shows the comparison of PSNR for different algorithms under the LOL dataset. Except for the method proposed, the PSNR of the other three algorithms fluctuates significantly under the LOL dataset. However, the maximum PSNR values for each algorithm are still obtained at a bit rate of 2000, which are 28.2db, 32.6db, 35.8db, and 37.1db, respectively. The maximum PSNR for the four algorithms has improved under the LOL dataset. A comparison was made between the brightness histograms of the low-light Chinese painting images enhanced by different algorithms and the brightness histogram of the original Chinese painting image, and the results are shown in Fig. 10.

In Fig. 10, Fig. 10(a) represents the brightness distribution histogram of the original low-light Chinese painting image. It can be seen that the high brightness region of the original image is concentrated in one area, and the brightness in other areas is at a lower level, indicating a highly uneven brightness distribution of the image. Fig. 10(b) represents the brightness distribution histogram after brightness equalization processing using the Zohair algorithm. It can be seen that the overall brightness of the image has significantly improved, but there are still some areas with low brightness values, indicating an uneven brightness distribution. Fig. 10(c) represents the brightness distribution histogram after brightness equalization processing using the algorithm proposed. The overall brightness of the image has significantly improved, and the brightness distribution is balanced in all parts, indicating that the proposed method can better perform brightness equalization processing on Chinese paintings captured in low-light environments.

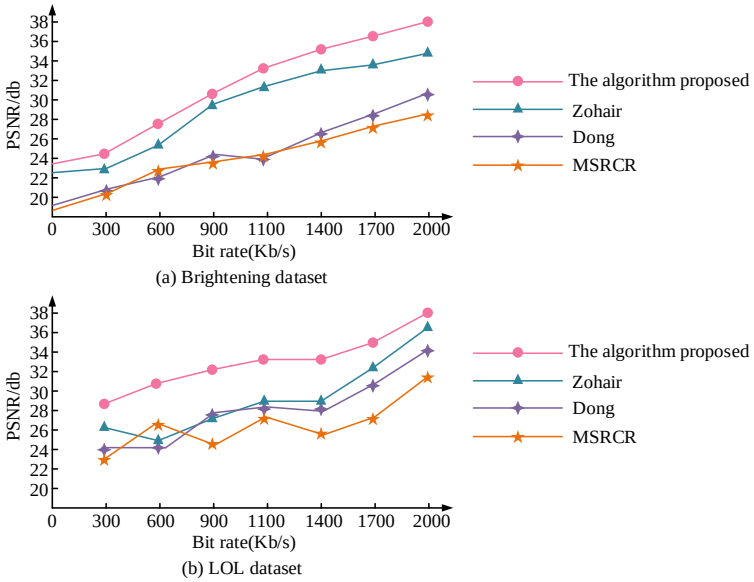

Fig. 9. Comparison of PSNR under different datasets.

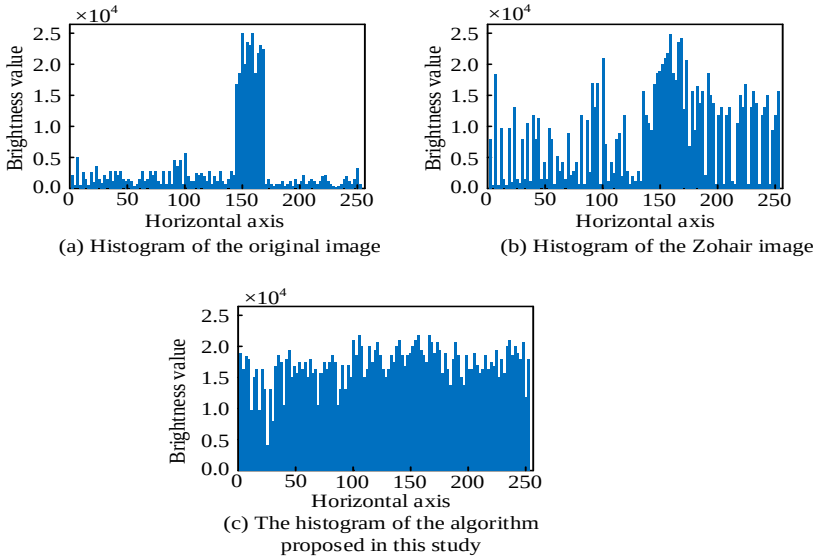

Fig. 10. Brightness histograms of low illuminance Chinese painting images enhanced by different algorithms.

V. CONCLUSION

The uneven display of pigment brightness in low light environments in Chinese painting poses certain obstacles to the promotion of Chinese painting and the dissemination of Chinese culture. Image denoising and image enhancement are common methods for processing low light images. However, traditional image denoising methods such as mean filtering and bilateral filtering may lead to loss of image details and poor generalization performance [21]. Traditional image enhancement methods based on grayscale transformation, histogram equalization, and Retinex theory also suffer from poor visual effects, unsatisfactory enhancement effects, and loss of details [22-23]. In this context, in order to enhance low light images more effectively, a region-based brightness equalization algorithm for low-light Chinese paintings was proposed. The performance test tells that the image information entropy enhanced by the proposed method was between 9 and 10, higher than the 5-7 of MSRCR, the 6-8 of Dong, and the 7-9 of Zohair, reaching the highest value among all the compared algorithms. This indicates that the image processed by the proposed algorithm presents more detailed information compared to other algorithms. The SSIM (Structural Similarity Index) of the image enhanced by the proposed method was between 0.30 and 0.36, significantly higher than the 0.06-0.23 of MSRCR, the 0.09-0.26 of Dong, and the 0.19-0.26 of Zohair. This indicates that the details of the image preserved after enhancement using the proposed method are more complete compared to other algorithms, resulting in better enhancement effects. In the simulation experiment, the brightness distribution histograms of the images after brightness equalization processing using different algorithms were compared. The testing outcomes tells that overall brightness value of the image processed by the proposed method was significantly improved compared to the original image. The brightness values were roughly between 1.51 and 2.0, indicating a more balanced distribution. This indicates that the proposed method can effectively perform brightness equalization processing for Chinese paintings in low-light environments. However, the proposed brightness equalization algorithm is easily affected by image brightness and noise when performing region partitioning, and it is implemented through simulation on the Matlab platform, which limits its runtime. Therefore, further research can explore better denoising methods for image preprocessing, algorithm optimization, and GPU acceleration.

REFERENCES

[1] Mishro P K, Agrawal S, Panda R, Abraham A. A novel brightness preserving joint histogram equalization technique for contrast enhancement of brain MR images. Biocybernetics and Biomedical Engineering, 2021, 41(2):540-553.

[2] Tirumani V H L, Tenneti M, Srikavya K C, Kotamraju S K. Image resolution and contrast enhancement with optimal brightness compensation using wavelet transforms and particle swarm optimization.IET image processing, 2021, 15(12):2833-2840.

[3] Jeevan K M, Anne G A B, Kumar P V. An image enhancement method based on gabor filtering in wavelet domain and adaptive histogram equalization. Indonesian Journal of Electrical Engineering and Computer Science, 2021, 21(1):146-153.

[4] Rao G S, Srikrishna A. Image Pixel Contrast Enhancement Using Enhanced Multi Histogram Equalization Method. Ingénierie des Systèmes D Information, 2021, 26(1):95-101.

[5] Hussain I, Muhammad J. Efficient convex region-based segmentation for noising and inhomogeneous patterns. Inverse Problems and Imaging, 2023, 17(3):708-725.

[6] Matsuyama E. A Novel Method for Automated Lung Region Segmentation in Chest X-Ray Images. Journal of biomedical science and engineering, 2021, 14(6):288-299.

[7] Chen Y, Gan H, Zeng Z, Chen H. DADCNet: Dual attention densely connected network for more accurate real iris region segmentation. International Journal of Intelligent Systems, 2021, 37(1):829-858.

[8] Cao R, Mo H, Gao C. Line Art Colorization Based on Explicit Region Segmentation. John Wiley & Sons, Ltd, 2021, 40(7):1-10.

[9] Tirumani V H L, Tenneti M, Srikavya K C, Kotamraju S K. Image resolution and contrast enhancement with optimal brightness compensation using wavelet transforms and particle swarm optimization.IET image processing, 2021, 15(12):2833-2840.

[10] Xu Y, Yang C, Sun B, Yan X, Chen M. A novel multi-scale fusion framework for detail-preserving low-light image enhancement. Information Sciences, 2021, 548(12):378-397.

[11] Liang Y. Analysis of the Integration of Chinese Painting Techniques in Watercolor Painting. Arts Studies and Criticism, 2022, 3(1):37-40.

[12] Lu B, Pang Z, Gu Y, Zheng Y. Channel splitting attention network for low-light image enhancement. IET Image Processing, 2022, 16(5):1403-1414.

[13] Reddy S K, Prasad R K. An Extended Fuzzy C-Means Segmentation for an Efficient BTD With the Region of Interest of SCP. International journal of information technology project management, 2021, 12(4):11-24.

[14] Wang W, Liu R. A saturation-value histogram equalization model for color image enhancement. Inverse Problems and Imaging, 2023, 17(4):746-766.

[15] Yu N, Li J, Hua Z. LBP-based progressive feature aggregation network for low-light image enhancement.IET image processing, 2022, 16(2):535-553.

[16] Choudhuri S, Adeniye S, Sen A. Distribution Alignment Using Complement Entropy Objective and Adaptive Consensus-Based Label Refinement for Partial Domain Adaptation. Artificial Intelligence and Applications. 2023, 1(1): 43-51.

[17] Yang Y, Song X. Research on face intelligent perception technology integrating deep learning under different illumination intensities. Journal of Computational and Cognitive Engineering, 2022, 1(1): 32-36.

[18] Ponmani E, Saravanan P. Image denoising and despeckling methods for SAR images to improve image enhancement performance: a survey. Multimedia Tools and Applications, 2021, 80(17): 26547-26569.

[19] Xu Y, Yang C, Sun B, Yan X, Chen M. A novel multi-scale fusion framework for detail-preserving low-light image enhancement. Information Sciences, 2021, 548(12):378-397.

[20] Sandoub G, Atta R, Ali H A, Abdel-KaderA R F. low-light image enhancement method based on bright channel prior and maximum colour channel. IET Image Processing, 2021, 15(8):1759-1772.

[21] Ilesanmi A E, Ilesanmi T O. Methods for image denoising using convolutional neural network: a review. Complex & Intelligent Systems, 2021, 7(5): 2179-2198.

[22] Hosny K M, Darwish M M, Aboelenen T. Novel fractional-order polar harmonic transforms for gray-scale and color image analysis. Journal of the Franklin Institute, 2020, 357(4): 2533-2560.

[23] Bulut F. Low dynamic range histogram equalization (LDR-HE) via quantized Haar wavelet transform. The Visual Computer, 2022, 38(6): 2239-2255.